

SUPPORTING INFORMATION

Kinetics of Self-Assembled Monolayer Formation on Individual Nanoparticles

Jeremy G. Smith^a and Prashant K. Jain^{a,b}*

^aDepartment of Chemistry, University of Illinois, Urbana Champaign, IL 61801 USA

^bMaterials Research Laboratory, University of Illinois, Urbana Champaign, IL 61801 USA

* *Corresponding Author E-mail: jain@illinois.edu*

Ag nanoparticle synthesis and characterization. Ag nanoparticles were synthesized according to a procedure developed in our laboratory. To a 20 mL scintillation vial containing 10 mL of deionized (DI) water (18.2 M Ω , Barnstead Nanopure), 25 μ L of 100 mM AgNO₃ (Amresco, 99.0%) and 25 μ L of 100 mM trisodium citrate (Alfa Aesar, 99.0%) were added. This solution was heated to 95 °C, in air, with stirring. 100 μ L of 20 mM sodium borohydride (J.T. Baker, 98%) was rapidly injected. The solution immediately turned yellow and remained that color. If the reaction temperature was too low, the solution color turned brown or black. Heating was maintained for 1 min, and then the solution was allowed to cool to room temperature. After 30 min, this solution of seed particles was stored in a refrigerator at 4 °C without purification. The seed solution stored in this manner is capable of being used for synthesis of high quality nanoparticles for at least 6 months.

In a 20-mL scintillation vial containing 10 mL of DI water (18.2 M Ω), 25 μ L of 100 mM AgNO₃ and 15 μ L of 100 mM trisodium citrate were added. To this solution, 50-400 μ L of the seed solution was added. Adding a smaller amount of seed solution resulted in larger nanoparticles, and red shifted spectra. With stirring, under air at room temperature, 15 μ L of 100 mM L-(+)-ascorbic acid (Alfa Aesar, 99%) was rapidly injected. The solution gradually changed color from faint yellow, to red, to purple, to blue. Following 30 min of stirring, the vial was removed and stored in the fridge. The solution was found to be stable over several months. All experiments for the current investigation were done with nanoparticles made with 300 μ L of the seed solution. Ensemble absorbance spectra and bright field transmission electron microscopy (BF-TEM) images of these nanoparticles are shown in Figures S1 and S2 respectively. Absorbance spectra were taken on a Shimadzu UV-3600 spectrophotometer with a 1-nm resolution at a fast scan speed. TEM was performed on a JEOL 2010 LaB₆ operating at 200 kV.

The sample was seen to consist of nanospheres and nanorods in addition to nanoplates. The nanoplates were seen to be single-crystalline with the face of nanoplates constituted by the (111) lattice plane of Ag (Figure S2 C, D). The nanorods were found to be single-crystalline with their long axis constituted by the (111) lattice plane of Ag (Figure S2 E, F). The nanospheres were seen to be polycrystalline (Figure S2 G, H).

Flow-cell preparation. All single-nanoparticle microscopy was carried out in home-built flow cells amenable to dark-field scattering microscopy. Flow cells were prepared immediately prior to use. Glass slides (76.2 mm x 25.4 mm and 1.2 mm thickness, VWR Vistavision) were drilled with a 1-mm diamond coated drill bit at ~20 kRPM under water. Using a 2.5-mm diamond coated drill at ~20 kRPM, a second hole was drilled ~50 mm away to serve as an outlet. Slides were cleaned by soaking in a 2M aqueous solution of NaOH for 30 min, thoroughly rinsed with DI water, sonicated for 10 min in DI water, and then rinsed again thoroughly with DI water. Coverslips (24 x 60 mm, No.1, VWR Superslip) were subjected to the same cleaning procedure. A drop (from a plastic pipette) of the undiluted Ag colloid solution was added to 2 drops of DI water in an Eppendorf tube and mixed. This solution was then drop cast onto the cleaned coverslip, and spread across the entire surfaces by tilting the coverslip. Since the coverslips are freshly cleaned the solution wets the surface very well. The excess liquid is wicked off onto a paper towel, leaving a thin layer of liquid on the surface. This thin layer is then blown off with pressurized air. This is found to leave behind a uniform coating of particles, sufficiently dispersed to allow single particle spectroscopy/microscopy. Polyethylene tubing (Instech Laboratories, 0.076 mm ID) was inserted into the 1-mm drilled hole and glued into place with 5 minute-epoxy (Loctite) and allowed to cure for at least 20 min. Double-sided tape (3M) placed along each long edge of the slide defined the height of the flow channel (tens of μm). Epoxy was

applied around the interior edges of the tape to create a liquid-tight seal and the nanoparticle coated cover slip was placed face down on top of the tape and gently pushed down so that the epoxy spread evenly. The cell was then allowed to dry for 30 min before imaging and spectroscopy were performed.

Single-nanoparticle microscopy. Dark-field scattering microscopy and spectroscopy was performed on an Olympus IX-51 microscope equipped with a U-LH100-3 100W halogen lamp source focused through an Olympus U-DCW 1.2-1.4 NA oil immersion dark field condenser and collection achieved via an Olympus UPlanApo 0.5-1.35 NA 100x oil immersion objective. A Princeton Instruments Acton spectrograph and a PyLoN 7570-0003 charge-coupled device (CCD) were used for acquiring spectral movies. Ag nanoparticles were immobilized on the surface of the glass cover slip of the flow cell. It was ensured that individual nanoparticles were well-separated from one other, such that they could be addressed individually, despite the diffraction-limited nature of the microscopy. A slit was inserted between the microscope light-output port and the spectrograph to isolate a handful of nanoparticles for spectroscopic acquisition. The signal was dispersed with a 300 g/mm grating, centered at 600 nm. Acquired spectra were corrected in real time by subtracting dark counts and dividing by the spectrum of the light source in WinSpec software.

For experiments with cleaned nanoparticles (main text figures, Figures S3-S5), deionized water, absolute ethanol and a solution containing varying concentrations of 1-dodecanethiol (>98%, Sigma-Aldrich) in ethanol were thoroughly deaerated by bubbling dry N₂ through these for 45 minutes. For performing microscopy, the flow cell was placed on top of the microscope objective, with the coverslip facing down towards the objective. Absolute ethanol was then injected into the cell with a plastic syringe. The flow cell was then flushed with ~0.5 mL of a

solution of either 1 mM or 0.2 mM NaBH₄ in deionized water. Following treatment with NaBH₄, the flow cells were flushed with 2 mL of the deaerated deionized water and then 2 mL of the deaerated ethanol. Once the cell had been flushed with ethanol, a septum was placed over the outlet to seal the cell. Then the syringe was replaced with one containing a freshly prepared ethanolic solution of DT. This was done in such a way as to leave a ~1 mm bubble in the tubing at the inlet. The purpose of the bubble is to prevent mixing of pure ethanol and the DT solution before entry of the fluid into the body of the cell. Often at the start of the imaging, often nanoparticles in the field-of-view were significantly out of focus. This defocus was corrected in due course before entry of the DT solution into the flow cell. The time-point when the DT solution entered the cell is set to $t = 0$ s in all figures. All experiments were performed with a KD Scientific syringe pump operating at a flow rate of 1.5 mL/hr. During the longest experiments (those performed with 1 μ M concentration of DT solution, which lasted more than 20 minutes), the objective focus was seen to drift, which was corrected manually.

For experiments with citrate-covered nanoparticle surfaces, a similar procedure was followed. Slides and coverslips were cleaned, casted and built into flow cells in the same manner. In this case, solutions were not deaerated with N₂. Instead a freshly prepared flow cell was rinsed first with 2 mL of deionized water and then with 2 mL of absolute ethanol. Subsequently, a syringe containing a solution of DT in ethanol was attached, again leaving a small bubble between the pure ethanol and the DT solution. Microscopy was performed in the same manner as described above. Results of these experiments are shown for comparison in Figure S6.

Data analysis

Single-nanoparticle spectra: From the acquired spectral movies, spectra as a function of time were extracted using Image J by selecting a square region of interest of 9 pixels around each nanoparticle. Manual processing of spectra from individual emitters allowed us to eliminate spectra from aggregates and nanoparticles that drift out of the spectrometer slit. Emitters with multiple peaks in their spectra were excluded from our analysis since these emitters are most likely aggregates of nanoparticles. Secondly, we eliminated from our analysis any nanoparticle that drifted outside of the slit, which was manifested as a dramatic and sudden decrease in the intensity of that particular nanoparticle. We also exclude cases where a nanoparticle exhibits a sudden increase in its intensity and a change in its spectral profile due to a new nanoparticle drifting into the slit and spatially overlapping with our chosen nanoparticle. Each single-nanoparticle spectrum in a movie was fit using a MATLAB code to a Lorentzian function of the form:

$$I = \frac{A_1}{(\lambda - \lambda_{max})^2 + A_2} + C$$

where λ_{max} defines the scattering peak maximum, A_1 and A_2 are related to the peak width, and C defines a baseline intensity for the spectrum.

Single-nanoparticle time-trajectories: The scattering spectrum red-shifts with increasing refractive index; therefore, the magnitude of the red-shift, normalized to the saturation value of the shift, was used as a measure of the extent of DT adsorption or self-assembled monolayer (SAM) formation. For each nanoparticle, the red-shift in λ_{max} (relative to the value of λ_{max} at $t =$

0) was determined as a function of time t . Time-trajectories of the red-shift, $\Delta\lambda_{max}$, were plotted for all single nanoparticles (Figure S5), with the time of entry of the DT solution into the flow cell set to $t = 0$ s. These plots of $\Delta\lambda_{max}$ vs. t were subsequently normalized to the magnitude of the shift at saturation coverage ($\Delta\lambda_{max,s}$) to obtain the trajectories plotted in Figure 3. $\Delta\lambda_{max,s}$ was obtained from fitting these single particle traces to monoexponential function of the form: $y = y_0 + Ae^{-t*k}$. Only the portion of the trajectory between the onset and the end of the trajectory was fit ($t = 35$ s for 10 and 1 mM, $t = 70$ s for 0.01 and 0.1 mM). The mono-exponential function yielded a good fit to the trajectories as confirmed by the value of R^2 of 0.75-0.99, with only 9 total traces less than 0.90 (Figure S4). The value of k obtained from a fit represents the rate constant for SAM formation with units of s^{-1} . y_0 values obtained from fits to un-normalized ensemble trajectories represent the LSPR shift in the limit of saturation coverage ($\Delta\lambda_{max,s}$). Normalization was performed to account for the fact that the magnitude of the total red-shift resulting from complete SAM formation is variable from one nanoparticle to another. This variation results from differences in the refractive index sensitivity of nanoparticles of different shapes, sizes, and/or orientations relative to the incident light. Variation also arises from differences in the SAM density from one nanoparticle to another.

Ensemble time-trajectories: In order to generate an ensemble-averaged time trajectory at each concentration of DT, we averaged normalized trajectories over several single nanoparticles. Each experimental trial yields typically only 4-6 single-nanoparticle trajectories. Therefore, in order to ensure reasonable statistics, single-nanoparticle trajectories from a several different trials at the same concentration were combined together. For DT concentrations of 10, 1, 0.1 and 0.01 mM, we averaged trajectories from 60, 39, 16 and 20 nanoparticles respectively (Figure 3) in order to generate the ensemble trajectories shown in Figure 4 A. Ensemble rate constants were obtained

by averaging all of the single nanoparticle rate constants shown in the histogram in Figure 4 B, similarly the ensemble-averaged $\Delta\lambda_{\max,s}$ was obtained by averaging the $\Delta\lambda_{\max,s}$ values from all of the single-nanoparticle trajectory fits at a given DT concentration.

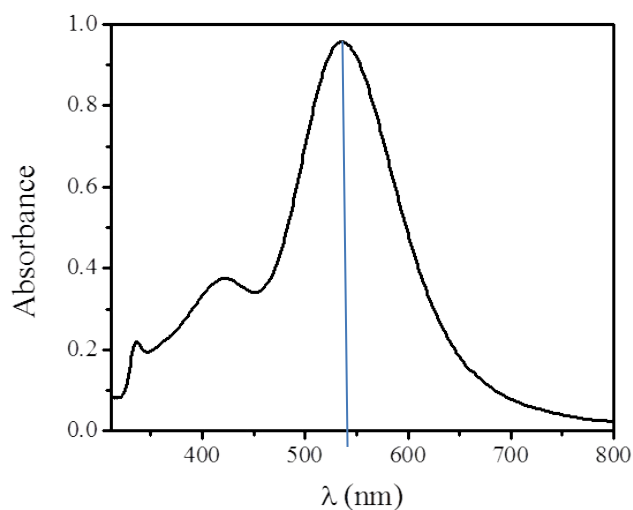


Figure S1. UV-Vis extinction spectrum of the Ag nanoparticle sample used in the experiments. Ag nanoparticles were made by a seed-mediated method developed in our laboratory, as detailed in SI text. The peak at ca. 540 nm is primarily from the in-plane dipolar LSPR mode of plate-like nanoparticles. However, this extinction spectrum only represents an average. The sample is heterogeneous and consists of spherical nanoparticles and nanorods in addition to nanoplates (Fig. S2). The LSPR maxima of individual nanoparticles can therefore range from 400-700 nm depending on shape. Our single-nanoparticle experiments are biased in favor of nanoparticles with redder LSPR maxima, because these nanoparticles also exhibit stronger scattering, which facilitates imaging. Secondly, the individual nanoparticles affixed to the glass slide ($n_{\text{glass}} = 1.5$) and immersed in ethanol ($n_{\text{EtOH}} = 1.361$) are subject to a higher effective medium RI as compared to the citrate-covered nanoparticles in aqueous solution ($n_{\text{water}} = 1.33$). Thus, the substrate-supported individual nanoparticles exhibit redder LSPRs than the peak maximum of the bulk, solution-phase extinction spectrum.

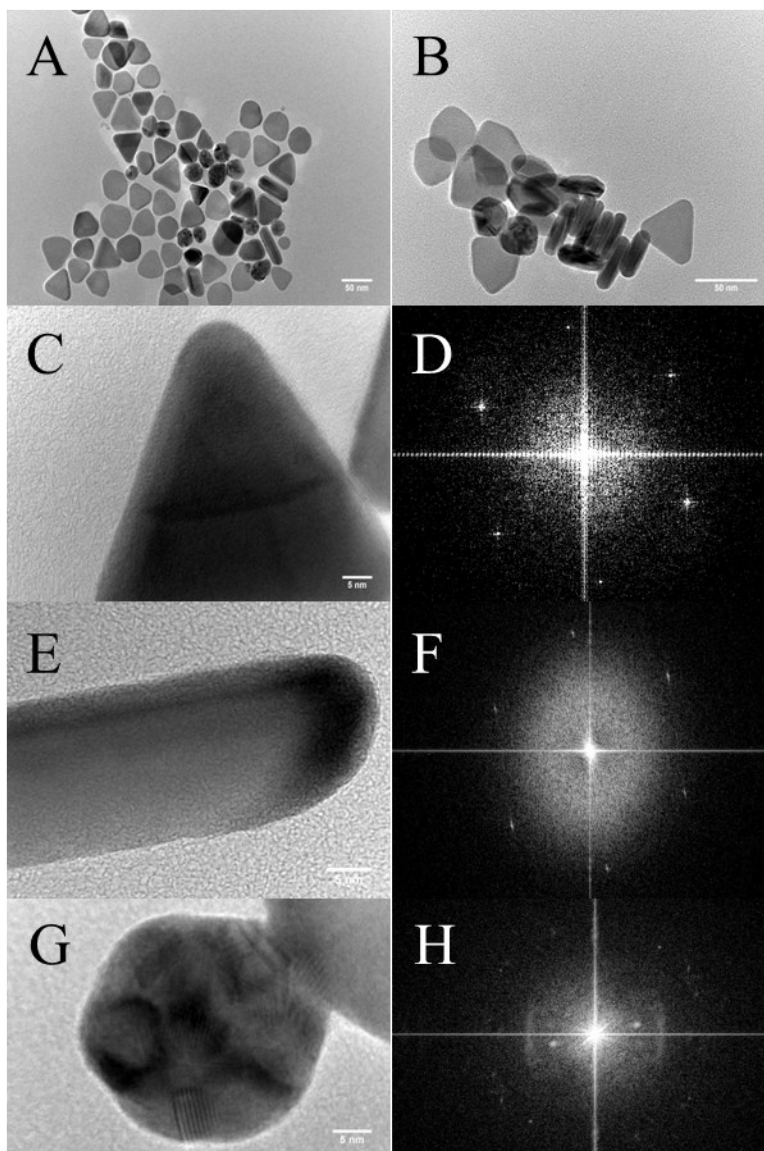


Figure S2. Representative bright-field TEM images (A and B) of a wide-field of Ag nanoparticles. The sample consists of nanospheres and nanorods in addition to nanoplates. High-resolution bright-field TEM image (C) of an individual nanoplate. A fast-Fourier transform (D) of the nanoplate shown in (C) yields discrete spots, indicating that the face of the nanoplate is single-nanocrystalline in nature and is constituted by the (111) lattice plane of Ag. High-resolution bright-field TEM image (E) of an individual nanorod. A fast-Fourier transform (F) of the nanorod shown in (E) yields discrete spots, indicating that the nanorod is single-crystalline in nature with its long axis constituted by the (111) lattice plane of Ag. High-resolution TEM image of an individual nanosphere (G). Several distinct domains can be observed in the image. A fast-Fourier transform (H) of the nanosphere shown in (G) has a series of spots that begin to constitute a diffraction ring, an indication of the polycrystallinity of the nanosphere.

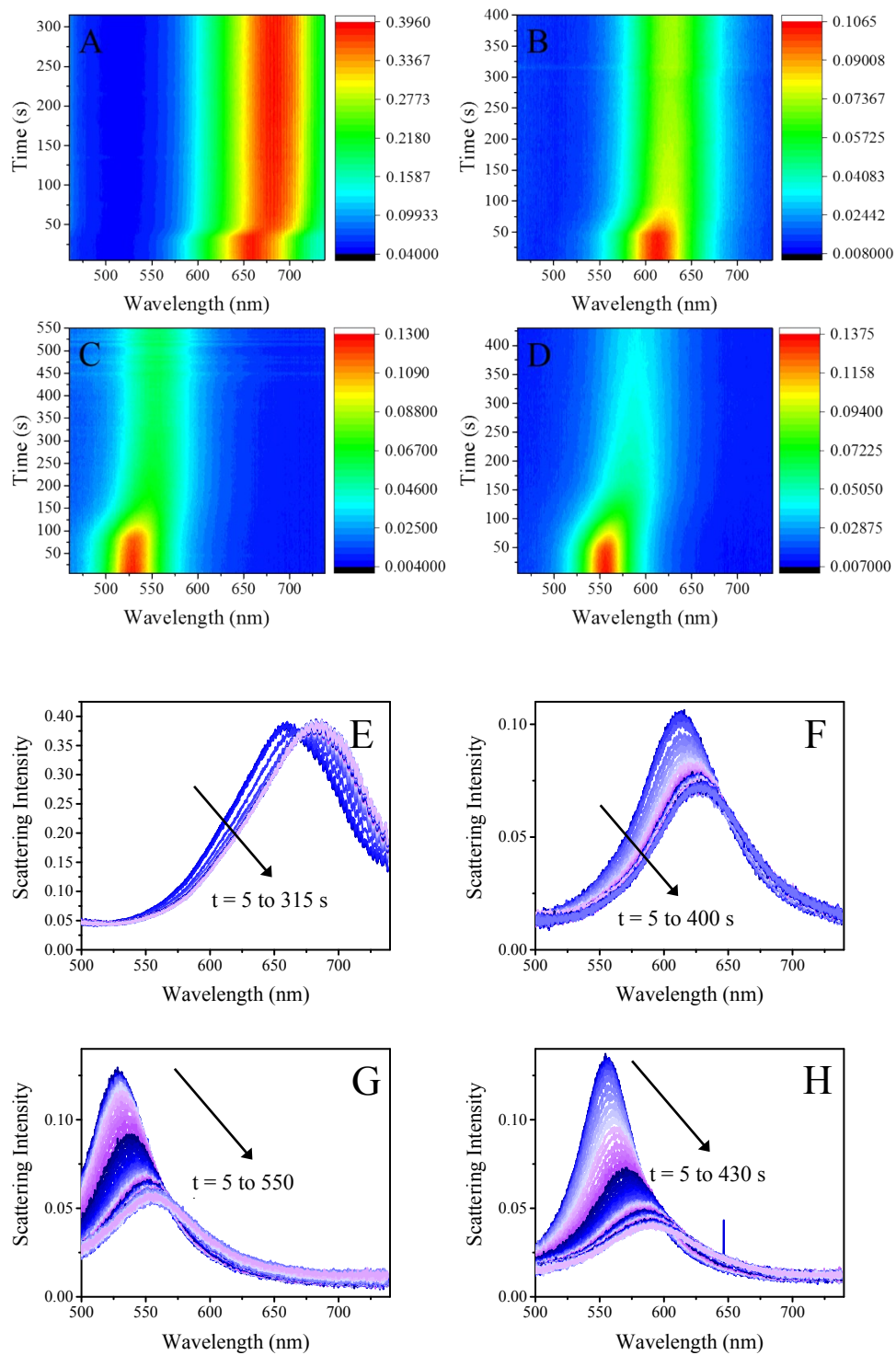


Figure S3. Time evolution of the LSPR scattering spectra of individual Ag nanoparticles in response to a 1.5 mL/hr flow of DT solution in ethanol at a concentration of 10 mM (A, E), 1 mM (B, F), 0.1 mM (C, G) and 0.01 mM (D, H). The DT solution enters the flow cell at $t = 0$ s in all cases. The adsorption of DT on the Ag nanoparticle surface induces a red shift of the LSPR

scattering spectrum, consistent with the higher refractive index of DT (1.459) relative to ethanol (1.361), the medium. Spectra were collected with a 5-s integration time. In the color contour plots (A-D), scattering intensity is represented on a color scale, with red denoting the highest intensity and black denoting the lowest intensity. In addition, we show in (E-H) scattering spectra as a function of time, corresponding to the contour plots in (A-D). These spectra show that, accompanied by the LSPR red-shift observed with time, there is considerable broadening and damping of the scattering spectrum, most likely owing to chemical interface damping resulting from the formation of Ag-S bonds. Such an effect was observed at the single-nanoparticle level by Orrit and coworkers.^{S1} It appears that the degree of damping and broadening is positively correlated with the magnitude of LSPR red-shift. This correlation supports the assignment that the damping and broadening have the same origin as the LSPR red-shift, i.e., thiol binding. It must be noted that the broadening and damping are not caused by structural changes to the nanoplates, such as rounding of tips and edges; such changes would cause a blue shift rather than a red-shift.

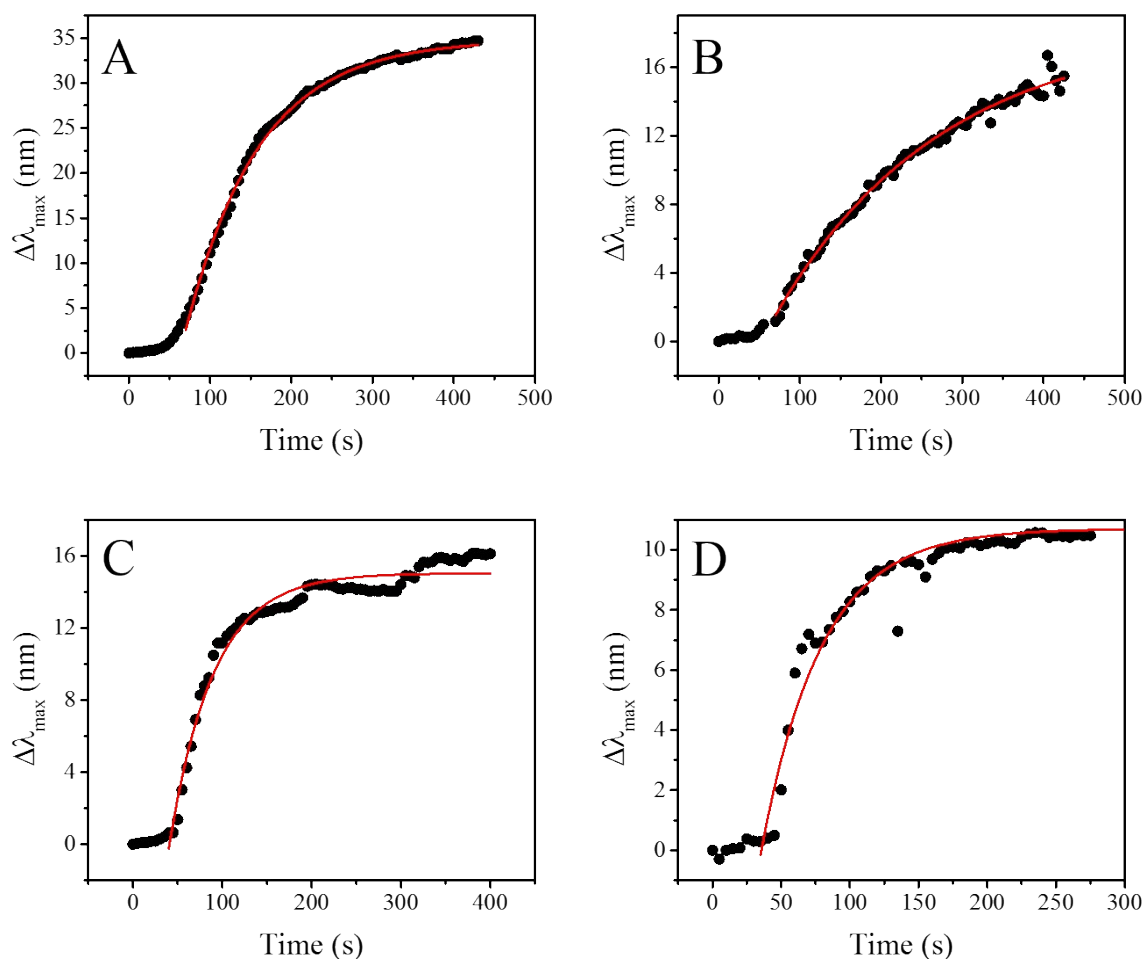


Figure S4. A representative single-nanoparticle trajectory (black dots) of SAM formation is shown at each one of the four concentrations of DT in ethanol: 10 mM (A), 1 mM (B), 0.1 mM (C) and 0.01 mM (D). These representative trajectories were selected from the full set of trajectories shown in Figure 3. For each representative trajectory, the fit of the kinetics to a mono-exponential function ($y = y_o + Ae^{-t*k}$) is shown by the red curve. Data-points prior to the onset of adsorption were ignored in the fitting. All single-nanoparticle trajectories, shown in Figure 3, appear to fit such a mono-exponential function. The goodness of the fits, indicated by an adjusted R² value, ranged from 0.75-0.99 with 9 trajectories with a value less than 0.90.

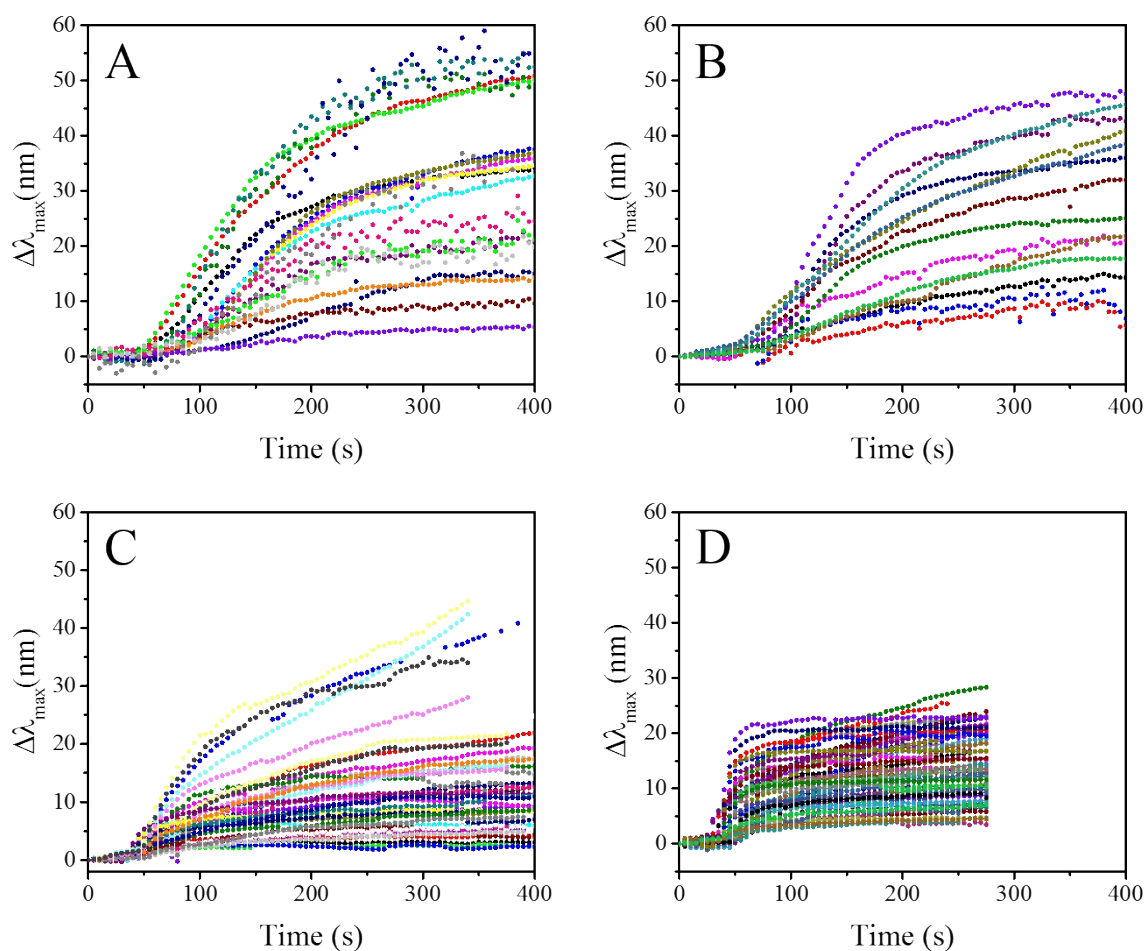


Figure S5. Entire set of single-nanoparticle trajectories at different concentrations of DT. Trajectories are shown for the entire set of 20 individual Ag nanoparticles at a concentration of 0.01 mM (A), 16 individual Ag nanoparticles at 0.1 mM (B), 39 individual Ag nanoparticles at 1 mM (C), and 60 individual Ag nanoparticles at 10 mM (D). The flow rate of the DT solution was 1.5 mL/hr at all concentrations. Entry of DT solution into the flow cell is set to $t = 0$ s. Trajectories shown here involve plots of LSPR shift versus time, whereas the normalized LSPR shift versus time is plotted in the trajectories shown in Figure 3.

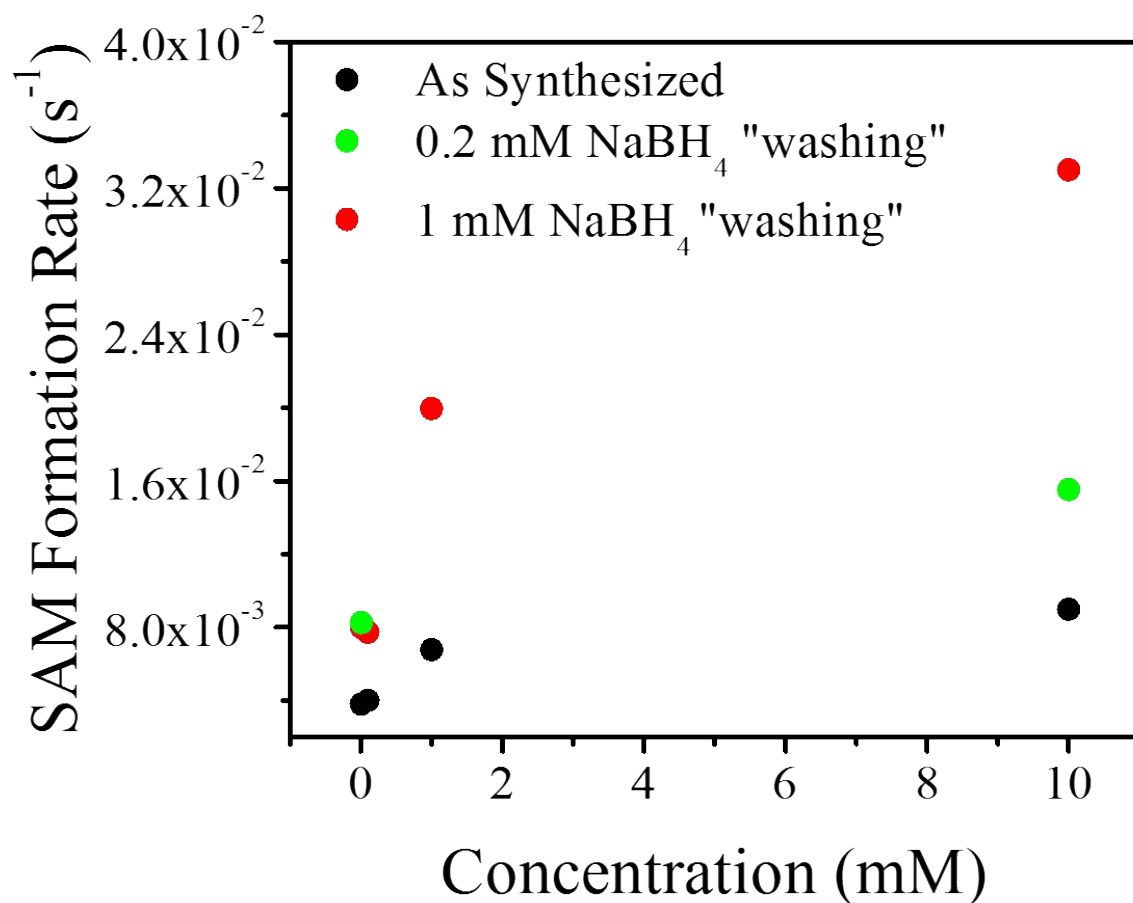


Figure S6. Effect of surface cleaning on the ensemble-averaged SAM formation rate. Single-nanoparticle trajectories of SAM formation for nanoparticles cleaned by washing with 1.0 mM NaBH₄, as well as those obtained with 0.2 mM NaBH₄ washing and those from uncleaned, as-synthesized citrate-covered nanoparticles were fit to a mono-exponential function. The ensemble-averaged SAM formation rate constant was obtained by averaging rate constants for all individual nanoparticles in an experiment. The ensemble-averaged SAM formation rate constant was found to be consistently higher for the cleaned nanoparticles at all DT concentrations.

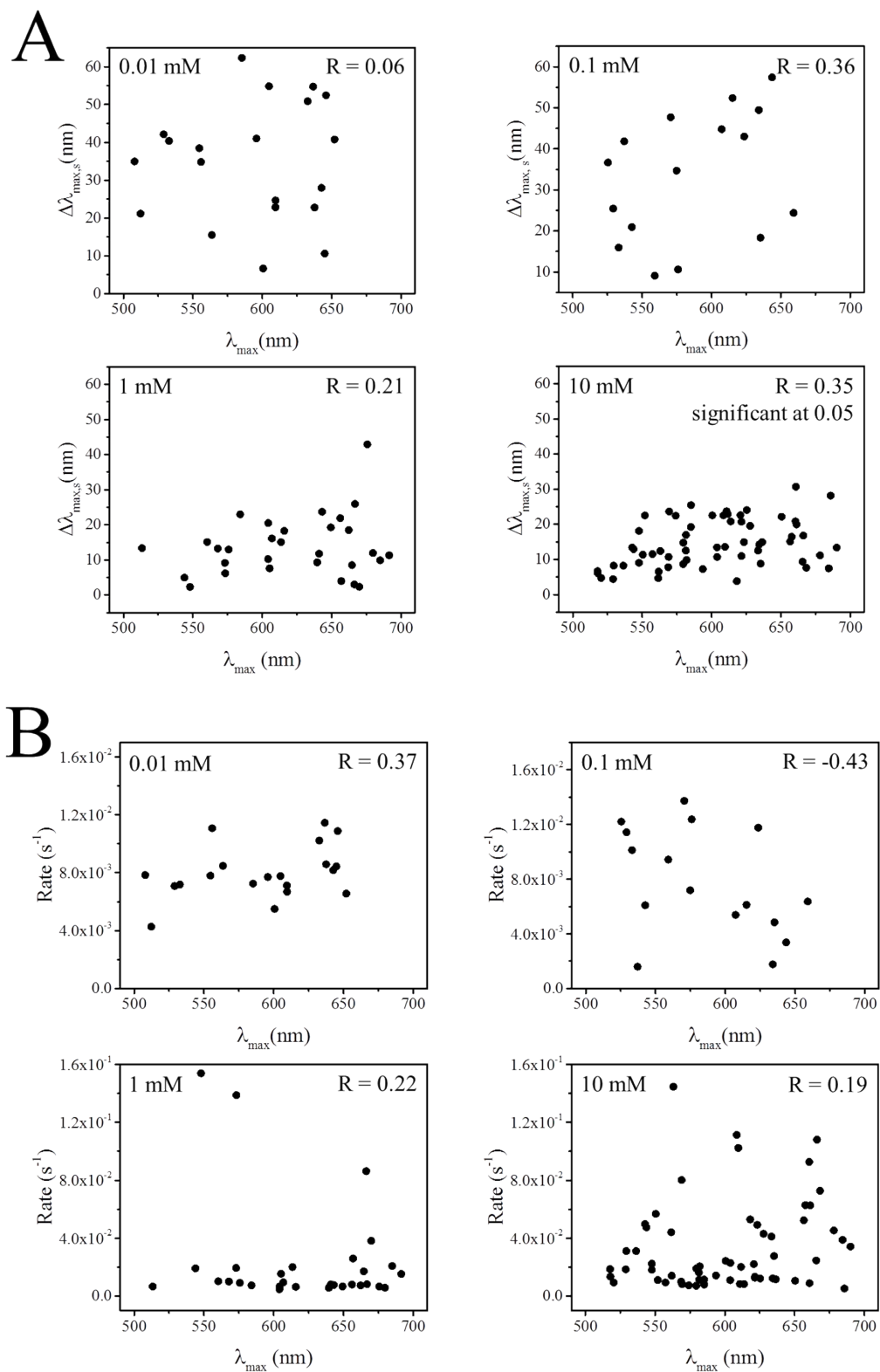


Figure S7. A) The saturation value of the LSPR shift, $\Delta\lambda_{\max,s}$ varied from nanoparticle to nanoparticle as seen in Fig. S5. Therefore, at each DT concentration, we plot for the single-nanoparticle population the correlation between $\Delta\lambda_{\max,s}$ and the initial LSPR maximum, λ_{\max} .

Since the nanoparticles are heterogeneous in shape, we conjectured that the variation in $\Delta\lambda_{\max,s}$ is a result of differences in nanoparticle shape or geometry. In the past it has been shown that anisotropic nanoparticles or those with high curvature surfaces exhibit a larger polarizability (or shape factor κ), as a result of which they have a greater RI sensitivity than more rounded nanoparticles.^{S2} At the same time, the LSPR maximum, λ_{\max} can be representative of the geometry of the nanoparticle. Anisotropic nanoparticles or those with high curvature surfaces exhibit redder maxima than more rounded nanoparticles. Both the RI sensitivity and the LSPR maximum depend in a similar way on the geometry of the nanoparticle via their dependence on the shape factor κ . Therefore, $\Delta\lambda_{\max,s}$ can be expected to correlate strongly with λ_{\max} . The degree of correlation, as indicated by the Pearson's correlation coefficient R , is either weak or low. There are some important issues responsible for the lack of a clear correlation. For single nanoparticles supported on substrates, there is an additional source of heterogeneity that can be quite dominant.^{S3} The degree of contact the nanoparticle has with the glass substrate can vary significantly. When all else is held constant, nanoparticles with a greater degree of contact with the high RI glass substrate ($n_{\text{glass}} \sim 1.5$) would have redder LSPR maxima, λ_{\max} . However, these nanoparticles would also exhibit a smaller saturation shift because the contact with the high RI glass would reduce the magnitude of the effective RI increase caused by SAM formation. This latter effect can nullify or weaken any positive correlation between $\Delta\lambda_{\max,s}$ and λ_{\max} resulting from geometric effects. Another complicating effect is the nanoparticle-to-nanoparticle variability in the packing density of the SAM, which also leads to differences in the saturation LSPR shift. The third source of variability is the surface cleanliness of the nanoparticles, which can influence the initial LSPR maximum, the quality of the SAM formed on the surface, and the magnitude of RI change and LSPR shift occurring upon saturation coverage.

B) As a coarse exploration of how the kinetics depends on the nanoparticle shape or faceting, we investigated if there is correlation between the SAM formation rate and the initial LSPR maximum, λ_{\max} , employed as a surrogate of the nanoparticle shape. Our prime interest was to determine whether anisotropic nanoparticles or those with highly curved surfaces (with redder λ_{\max}) exhibit rates appreciably different from more rounded nanoparticles (with bluer λ_{\max}). But the Pearson's R values, at different concentrations, show the lack of a clear correlation. This does not mean that shape does not play a role; rather the effect of shape on kinetics is likely shrouded by other factors. As shown in Fig. S6, surface cleanliness is a critical factor in the SAM formation kinetics. The average SAM formation rate at 10 mM DT is four-fold higher for nanoparticles cleaned using 1 mM NaBH_4 than for uncleaned, citrate-covered nanoparticles. The degree of surface cleanliness (i.e., the presence of adsorbed impurities, oxide layer, and remnant citrate molecules that need to be displaced by thiol) can vary from one nanoparticle to another, thereby leading to considerable variability in the SAM formation rate. This effect can easily complicate or overshadow any dependence of the rate on the nanoparticle shape, size, or faceting. In fact, a recent study from our group has found that surface adsorbates can play a much more dominant role in the kinetics of surface reactions than factors such as nanoparticle size or shape.^{S4}

SUPPORTING INFORMATION REFERENCES

S1) Zijlstra, P.; Paulo, P. M. R.; Yu, K.; Xu, Q.-H.; Orrit, M. *Angew. Chem. Int. Ed.* **2012**, *51* (33), 8352-8355.

S2) Jain, P. K.; El-Sayed, M. A. *J. Phys. Chem. C* **2007**, *111* (47), 17451–17454.

S3) Mock, J. J.; Smith, D. R.; Schultz, S. *Nano Lett.* **2003**, *3* (4), 485-491.

S4) Smith, J. G.; Jain, P. K. *J. Am. Chem. Soc.* **2016**, *138* (21), 6765–6773.